JAK2-V617F promotes venous thrombosis through β_1/β_2 integrin activation

Bärbel Edelmann,[1,2] Nibedita Gupta,[1,2] Tina M. Schnoeder,[1,3,4] Anja M. Oelschlegel,[5,6] Khurrum Shahzad,[7] Jürgen Goldschmidt,[5] Lars Philipsen,[2,8] Soenke Weinert,[2,9] Aniket Ghosh,[5] Felix C. Saalfeld,[1,2] Subbaiah Chary Nimmagadda,[1,2] Peter Müller,[1,2] Rüdiger Braun-Dullaeus,[2,9] Juliane Mohr,[2,8] Denise Wolleschak,[1,2] Stefanie Kliche,[2,8] Holger Amthauer,[10] Florian H. Heidel,[1,3,4] Burkhart Schraven,[2,8,11] Berend Isermann,[2,7] Andreas J. Müller,[2,8,11] and Thomas Fischer[1,2]

[1]Department of Hematology and Oncology, Medical Center, Otto-von-Guericke University, Magdeburg, Germany. [2]Gesundheitscampus Immunologie, Infektiologie und Inflammation (GCI[3]), Medical Center, Otto-von-Guericke University, Magdeburg, Germany. [3]Internal Medicine II, Hematology and Oncology, University Hospital Jena, Jena, Germany. [4]Leibniz Institute on Aging, Fritz-Lipmann-Institute, Jena, Germany. [5]Leibniz Institute for Neurobiology, Magdeburg, Germany. [6]Institute of Anatomy, [7]Institute of Clinical Chemistry and Pathobiochemistry, [8]Institute of Molecular and Clinical Immunology, and [9]Department of Cardiology and Angiology, Medical Center, Otto-von-Guericke University, Magdeburg, Germany. [10]Department of Radiology and Nuclear Medicine, University Hospital, Magdeburg, Germany. [11]Helmholtz Centre for Infection Research, Department of Immune Control, Braunschweig, Germany.

JAK2-V617F–positive chronic myeloproliferative neoplasia (CMN) commonly displays dysfunction of integrins and adhesion molecules expressed on platelets, erythrocytes, and leukocytes. However, the mechanism by which the 2 major leukocyte integrin chains, β_1 and β_2, may contribute to CMN pathophysiology remained unclear. β_1 ($\alpha_4\beta_1$; VLA-4) and β_2 ($\alpha_L\beta_2$; LFA-1) integrins are essential regulators for attachment of leukocytes to endothelial cells. We here showed enhanced adhesion of granulocytes from mice with JAK2-V617F knockin (JAK2$^{+/VF}$ mice) to vascular cell adhesion molecule 1– (VCAM1-) and intercellular adhesion molecule 1–coated (ICAM1-coated) surfaces. Soluble VCAM1 and ICAM1 ligand binding assays revealed increased affinity of β_1 and β_2 integrins for their respective ligands. For β_1 integrins, this correlated with a structural change from the low- to the high-affinity conformation induced by JAK2-V617F. JAK2-V617F triggered constitutive activation of the integrin inside-out signaling molecule Rap1, resulting in translocation toward the cell membrane. Employing a venous thrombosis model, we demonstrated that neutralizing anti–VLA-4 and anti–β_2 integrin antibodies suppress pathologic thrombosis as observed in JAK2$^{+/VF}$ mice. In addition, aberrant homing of JAK2$^{+/VF}$ leukocytes to the spleen was inhibited by neutralizing anti-β_2 antibodies and by pharmacologic inhibition of Rap1. Thus, our findings identified cross-talk between JAK2-V617F and integrin activation promoting pathologic thrombosis and abnormal trafficking of leukocytes to the spleen.

Introduction

Chronic myeloproliferative neoplasia (CMN) is a malignant hematopoietic disease characterized by excessive proliferation of one or more myeloid cell lineages as erythrocytes, platelets, or leukocytes. CMN comprises several sub-entities, including polycythemia vera (PV), essential thrombocytosis (ET), primary myelofibrosis (PMF), and others. Genomic analysis of CMN revealed an activating somatic point mutation of the *JAK2* gene (JAK2-V617F) in the majority (95%) of PV patients and in 50% of ET and PMF patients, respectively (1–3). JAK2-V617F–mutated CMN (PV, ET, and PMF) is driven by clonal proliferation of myeloid cells. Patients may develop an inflammatory syndrome consisting of fever, night sweats, and elevated serum proinflammatory cytokine levels (4, 5). Clinical studies using JAK kinase inhibitors have shown improvement of splenomegaly, systemic inflammatory symptoms, and overall survival (4–6). Venous and arterial thrombosis is the major cause of morbidity and mortality in PV and ET patients (7, 8). Strikingly, the thrombotic risk in these patients is dramatically higher than in patients with secondary erythrocytosis or thrombocytosis. This indicates that disease-intrinsic factors play a major role. Indeed, it has been reported that JAK2-V617F leads to abnormal function of erythrocytes and platelets (9, 10). Aberrant single-cell cytokine secretion (11) and elevated α_M integrin CD11b expression have been described in circulating granulocytes in PV, ET, and MF patients (12–14). Recently, our group has demonstrated that JAK2-V617F activates β_1 integrin–mediated adhesion of granulocytes isolated from CMN patients to vascular cell adhesion molecule 1 (VCAM1) (15). VCAM1 is expressed on venous endothelial cells and acts in leukocyte–endothelial cell adhesion (16, 17). However, the functional role of leukocyte integrins in the pathophysiology of JAK2-V617F–positive disease, in particular thrombosis and formation of splenomegaly, is still poorly defined. There is a large body of evidence showing that activation of integrins on leukocytes, in particular of β_1 and β_2 integrins, is fundamental to the process of leukocyte adhesion, migration,

▶ Related Commentary: p. 4248

Conflict of interest: BE and TF submitted a patent application related to compounds for the treatment of JAK2-V617F–associated chronic myeloproliferative neoplasia (European Patent Office application MKEY).
Submitted: August 30, 2016; **Accepted:** July 3, 2018.
Reference information: *J Clin Invest.* 2018;128(10):4359–4371.
https://doi.org/10.1172/JCI90312.

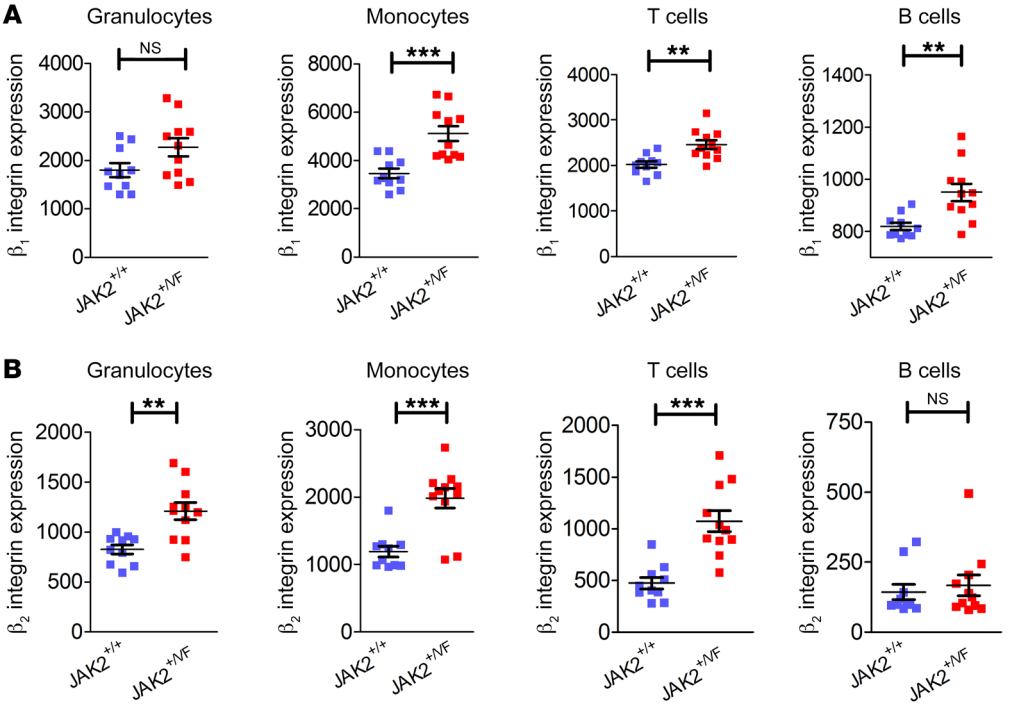

Figure 1. β_1 and β_2 integrin expression in the myeloid and lymphoid compartments of the bone marrow of JAK2$^{+/+}$ and JAK2$^{+/VF}$ mice. (**A**) β_1 integrin (CD29) expression and (**B**) β_2 integrin (CD18) expression in the myeloid (granulocytes and monocytes) and lymphoid (T and B cells) compartments of 10- to 12-week-old JAK2$^{+/+}$ (n = 10) and JAK2$^{+/VF}$ (n = 11) mice. Data are shown as mean ± SEM. $^{**}P \le 0.01$, $^{***}P \le 0.001$ (unpaired, 2-tailed Student's t test).

and inflammation (18–23). Two major integrin β-chains, β_1 and β_2, are expressed on leukocytes, forming either VLA-4 (very late antigen–4) or LFA-1 (lymphocyte function–associated antigen–1) (19). Unstimulated, VLA-4 and LFA-1 harbor a closed, inactive conformation, but in response to external stimuli (e.g., chemokines such as SDF1α) these integrins rapidly undergo a conformational change. This enhances both the affinity and the avidity for their natural ligands, VCAM1 or intercellular adhesion molecule 1 (ICAM1), which are typically expressed on endothelial cells and on cells of the immune system (24). The intracellular signaling processes controlling integrin activation are known as inside-out signaling (19) and include PI3K, phospholipase C (PLC), calcium diacylglycerol guanine nucleotide exchange factors (CalDAG-GEFs), small GTPases such as Rap1, adhesion- and degranulation-promoting adaptor protein (ADAP), and others.

It has long been suggested that leukocytosis is a potential thrombotic risk factor in PV and ET patients (8). The proposed pathophysiological mechanism includes abnormal interaction of leukocytes, especially neutrophils with platelets and endothelial cells (8, 25, 26). In PV and ET patients, markers of increased basal activation of neutrophils have been detected, including elevated expression of CD11b and increased levels of neutrophil proteases in the plasma, both of which exert prothrombotic activity (13, 26–28). The contribution of neutrophils to pathological venous thrombosis has been appreciated only recently, but is now recognized as being crucial for thrombus initiation and progression (29). Formation of neutrophil extracellular traps (NETs) contributes to coagulation and platelet aggregation (29, 30). In a model of deep vein thrombosis (DVT) applying partial ligation of the inferior vena cava (IVC), within only 1 hour of depressed venous blood flow, leukocytes started to roll along, adhere, or crawl on the venous endothelium (30). β_1 and β_2 integrins are essential in mediating rolling and firm adhesion of leukocytes to the endothelial layer, transmigration across the physical endothelium/extracellular matrix (ECM) barrier, and homing of leukocytes into tissues (18–23). We hypothesized that abnormal function of integrins on leukocytes, in particular neutrophils, may induce abnormal leukocyte-endothelium interaction and thus may contribute to pathologic thrombosis in CMN. In addition, abnormal trafficking of hematopoietic progenitors from bone marrow into the bloodstream and abnormal homing of hematopoietic cells including leukocytes to the spleen have been described as a prominent feature of JAK2-V617F–positive CMN (4, 5, 31–35). Using in vitro and in vivo experimentation, we sought to elucidate the role of abnormal β_1/β_2 integrin activity in the JAK2-V617F kinase–induced prothrombotic state and in aberrant homing of leukocytes to the spleen.

Results

Expression levels of β_1 and β_2 integrins in the hematopoietic system of JAK2$^{+/VF}$ mice. To investigate the effects of physiological JAK2-V617F expression on β_1 and β_2 integrin abundance, we used a JAK2-V617F–knockin mouse CMN model (36). Floxed heterozygous JAK2-V617F (JAK2$^{+/floxP\text{-}VF\text{-}floxP}$) mice were crossed with transgenic VavCre mice (JAK2$^{+/VF}$), resulting in JAK2-V617F protein expression in hematopoiesis. The resulting phenotype is characterized by an elevated hematocrit and WBC count, splenomegaly, and prominent splenic extramedullary hematopoiesis (Supplemental Figure 1, A–C; supplemental material available online with this article; https://doi.org/10.1172/JCI90312DS1), closely corresponding to data published earlier (36) and resembling human PV.

Expression levels of the 2 most prominent leukocyte integrins, β_1 and β_2, were analyzed in the myeloid and lymphoid compartments of the bone marrow of JAK2$^{+/+}$ (Cre$^+$) and JAK2$^{+/VF}$ (Cre$^+$) mice. β_1 (CD29) integrin expression was unchanged in granulocytes of JAK2$^{+/VF}$ compared with JAK2$^{+/+}$ mice, corroborating previously published results in human granulocytes isolated from JAK2-

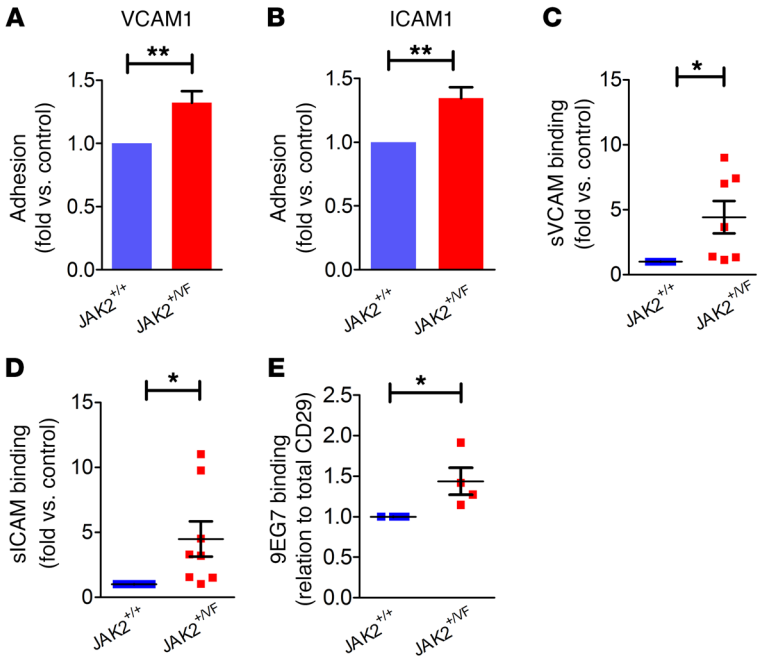

Figure 2. β_1 and β_2 integrins are activated on murine granulocytes. (**A** and **B**) Static adhesion of murine granulocytes isolated from 10- to 12-week-old JAK2$^{+/+}$ (n = 5) and JAK2$^{+/VF}$ (n = 5) mice on Fc-free VCAM1 (**A**) and ICAM1 (**B**). (**C**) Soluble VCAM1 (sVCAM1) binding assay of JAK2$^{+/+}$ (n = 7) and JAK2$^{+/VF}$ (n = 7) murine granulocytes. (**D**) Soluble ICAM1 (sICAM1) binding assay of JAK2$^{+/+}$ (n = 7) and JAK2$^{+/VF}$ (n = 8) murine granulocytes. (**E**) 9EG7 binding of JAK2$^{+/+}$ (n = 4) and JAK2$^{+/VF}$ (n = 4) murine granulocytes. Data are shown as mean ± SEM. *$P \le 0.05$, **$P \le 0.01$ (unpaired, 2-tailed Student's t test).

V617F–positive patients (15). Interestingly, in monocytes, T cells, and B cells, expression of β_1 integrins was upregulated, with the effect most prominent in monocytes (Figure 1A), indicating a differential regulatory mechanism of β_1 integrin expression in these cell types. In parallel, the expression levels of β_2 integrins (CD18) were found to be increased in granulocytes, monocytes, and T cells but not in B cells (Figure 1B). In a transplantation model wherein retrovirally transduced bone marrow cells expressing either JAK2-WT or JAK2-V617F were injected into lethally irradiated BALB/c mice, CD29 expression was unchanged in granulocytes, while CD18 expression was upregulated in the JAK2-V617F background (our unpublished observations), confirming the results obtained in the VavCre-JAK2-V617F knockin mouse model.

β_1 and β_2 integrin activity is enhanced in primary murine JAK2$^{+/VF}$ granulocytes and is dependent on Rap1-GTPase activity. Recently, we showed that human granulocytes from JAK2-V617F–positive patients have increased adhesion on a surface coated with the β_1 integrin ligand VCAM1 (15). Using primary granulocytes isolated from the bone marrow of JAK2$^{+/+}$ or JAK2$^{+/VF}$ mice, we performed static adhesion assays on VCAM1 or ICAM1 (ligand for β_2 integrins). Increased adhesion of JAK2$^{+/VF}$ granulocytes was detected on VCAM1 as well as on ICAM1 (Figure 2, A and B). Soluble ligand binding assays for VCAM1 (sVCAM1) and ICAM1 (sICAM1) revealed increased binding to JAK2$^{+/VF}$ granulocytes as compared with JAK2$^{+/+}$ cells (Figure 2, C and D). In addition, employing overexpression of JAK2-WT or JAK2-V617F in a Ba/F3 cell reconstitution model confirmed increased static adhesion on VCAM1 and ICAM1 of JAK2-V617F cells (Supplemental Figure 2, A and B). Again, soluble ligand binding revealed increased binding of VCAM1 (Supplemental Figure 2C).

To analyze the conformation status of β_1 integrins on granulocytes in JAK2$^{+/VF}$ and JAK2$^{+/+}$ mice, we tested 9EG7 antibody binding (Figure 2E). We found that JAK2$^{+/VF}$ granulocytes showed increased binding of 9EG7 antibody, indicating that β_1 integrins have shifted from the bent, low-affinity status to an open, high-affinity conformation.

Having demonstrated that β_1 and β_2 integrin activity is increased in JAK2$^{+/VF}$ granulocytes, we evaluated inside-out signaling of integrins. Rap1-GTPase was recently identified to be constitutively activated in JAK2-V617F–positive human granulocytes and directly involved in activation of β_1 integrins (15). Analysis of JAK2$^{+/+}$ and JAK2$^{+/VF}$ granulocytes confirmed increased activation of Rap1 in JAK2-V617F–mutated mice (Figure 3A). In contrast, in granulocytes of calreticulin-mutated (CALR-mutated) patients, Rap1 was activated to a minor degree only as compared with cells from JAK2-V617F–positive patients (Supplemental Figure 3A). This also applies to ERK phosphorylation in the presence of CALR mutation (Supplemental Figure 3B). To define the biological significance of this observation requires further investigation in a larger number of patients. However, it is tempting to speculate that differential ERK signaling and differential RAP1 activation may result in reduced β_1/β_2 integrin activation in CALR-mutated granulocytes. Interestingly, in view of the proposed role of β_1/β_2 integrin activation in thrombosis described below, the thrombotic risk in CALR-mutated ET patients was reported to be markedly reduced in comparison to those with JAK2-V617F–positive ET (37).

A large body of evidence from T cell studies suggests that activation of Rap1-GTP in control of β_1 integrin function is associated with translocation of the protein to the plasma membrane (38). To investigate whether JAK2-V617F kinase causes membrane relocalization of Rap1, we employed the 32D myeloid progenitor cell model ectopically expressing the erythropoietin receptor (Epo-R) and either JAK-WT or JAK2-V617F mutant (15, 39). Previously, we demonstrated that 32D JAK2-V617F cells display a strong increase in static adhesion to immobilized VCAM1 (the ligand for β_1 integrin VLA-4) but not to immobilized BSA (15). The presence of the mutated JAK2 compared with the JAK2-WT molecule in 32D cells resulted in increased localization of Rap1 in cytoplasm and translocation toward cortical actin (Figure 3B and Supplemental Figure 4). Plasma membrane isolation (Figure 3C) confirmed that constitutive activation of Rap1 in JAK2-V617F–mutated cells was indeed associated with translocation to the plasma membrane. Incubation with the geranylgeranyltransferase inhibitor GGTI-2147, which blocks posttranslational modifications of Rap1 required for activation and translocation to the plasma membrane (40), revealed a strong decrease in static adhesion on VCAM1 of JAK2$^{+/VF}$ granulocytes, while JAK2$^{+/+}$ granulocytes were largely unaffected (Figure 3D). This suggests that posttranslational processing of Rap1 is required for JAK2-V617F–induced integrin activation.

JAK2-V617F–induced Rap1 activation is mediated by PI3K and CalDAG-GEFI. Downstream of JAK2 kinase, PI3K and MAPK

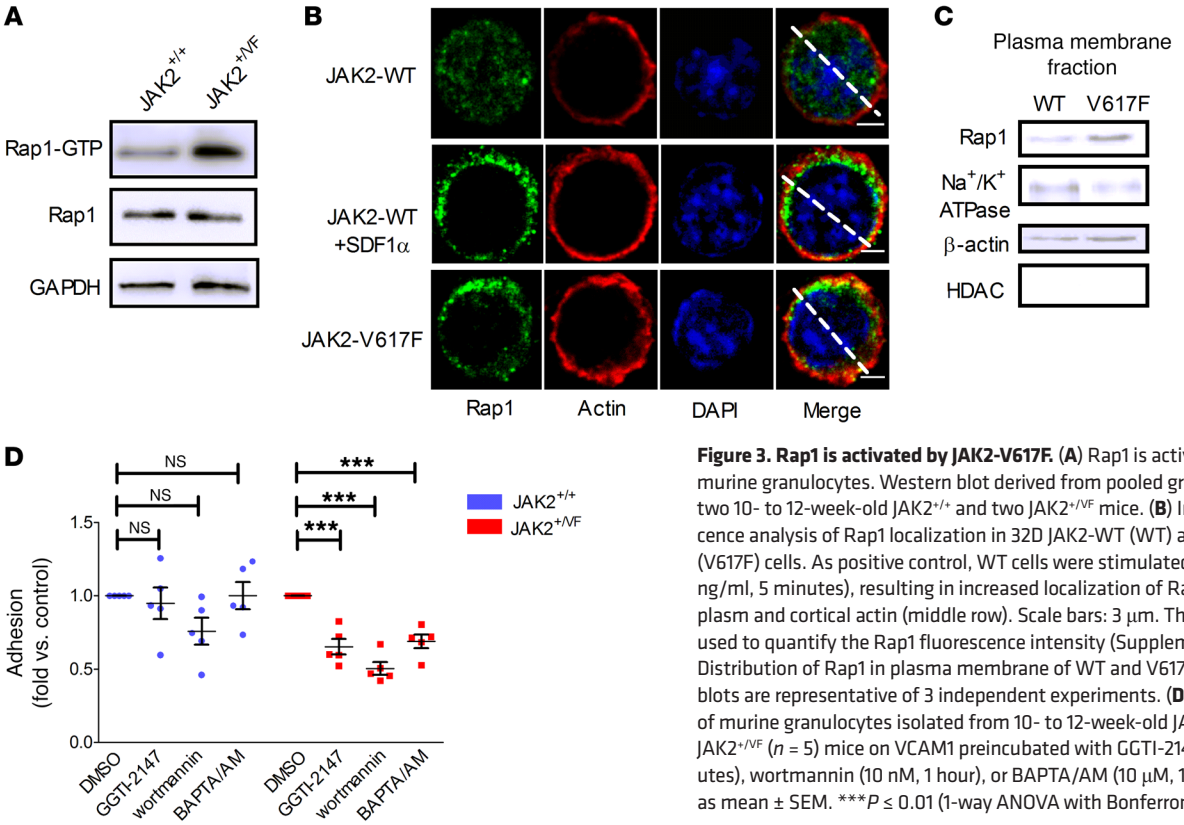

Figure 3. Rap1 is activated by JAK2-V617F. (**A**) Rap1 is activated in JAK2$^{+/VF}$ murine granulocytes. Western blot derived from pooled granulocytes from two 10- to 12-week-old JAK2$^{+/+}$ and two JAK2$^{+/VF}$ mice. (**B**) Immunofluorescence analysis of Rap1 localization in 32D JAK2-WT (WT) and JAK2-V617F (V617F) cells. As positive control, WT cells were stimulated with SDF1α (500 ng/ml, 5 minutes), resulting in increased localization of Rap1 toward cytoplasm and cortical actin (middle row). Scale bars: 3 μm. The white line was used to quantify the Rap1 fluorescence intensity (Supplemental Figure 4). (**C**) Distribution of Rap1 in plasma membrane of WT and V617F cells. Immunoblots are representative of 3 independent experiments. (**D**) Static adhesion of murine granulocytes isolated from 10- to 12-week-old JAK2$^{+/+}$ (n = 5) and JAK2$^{+/VF}$ (n = 5) mice on VCAM1 preincubated with GGTI-2147 (10 μM, 30 minutes), wortmannin (10 nM, 1 hour), or BAPTA/AM (10 μM, 1 hour). Data shown as mean ± SEM. ***$P \le 0.01$ (1-way ANOVA with Bonferroni's post test).

are activated, resulting in increased proliferation of JAK2-V671F–mutated cells (41). JAK$^{+/VF}$ granulocytes preincubated with the PI3K inhibitor wortmannin showed reduced adhesion on VCAM1 compared with JAK2$^{+/+}$ granulocytes (Figure 3D). This result was confirmed in 32D JAK2-V617F cells incubated with wortmannin (Figure 4A) and LY294002 (Figure 4B). Of note, in 32D JAK2-WT cells, adhesion on VCAM1 upon wortmannin treatment was only slightly reduced, and it was unchanged upon LY294002 treatment (Figure 4, A and B). LY294002-treated 32D JAK-V617F cells revealed reduced levels of active Rap1-GTP (Figure 4C), confirming an involvement of PI3K in the activation pathway of Rap1. However, it appears that Akt is not involved, since direct blockade of Akt by Akt inhibitor VIII did not alter adhesion or Rap1 activation (Figure 4D). For efficient conversion of Rap1-GDP to Rap-GTP, guanine exchange factors such as Epac, C3G, or CalDAG-GEFI are required (42–44). The incubation of JAK2$^{+/VF}$ granulocytes with the Ca^{2+} and Mg^{2+} chelator BAPTA/AM resulted in reduced adhesion to VCAM1 in comparison to JAK2$^{+/+}$ granulocytes (Figure 3D). The results were confirmed in 32D JAK2-V617F and JAK2-WT cells (Figure 4E), suggesting a Ca^{2+}-dependent activation pathway.

Since CalDAG-GEFI is a Ca^{2+}-dependent enzyme, knockdown of CalDAG-GEFI using shRNA was performed in 32D JAK2-V617F cells. Adhesion to VCAM1 was reduced, albeit to a minor degree (Figure 4, F and G). Together, these results suggest that PI3K and CalDAG-GEFI signaling contribute to Rap1 activation and to increased adhesiveness of JAK2-V617F–positive cells.

Blockade of β_1 and β_2 integrin activity suppresses pathologic thrombus formation in a thrombosis model using JAK2$^{+/VF}$ mice. Thrombotic events are the major cause for morbidity and mortality in JAK2-V617F–positive PV and ET. Neutrophils, monocytes, and platelets cooperate to initiate and propagate venous thrombosis in mice in vivo (30). Interestingly, neutrophils constitute the major leukocyte subset and play a dominant role during the early phase of venous thrombosis (30). Blood flow restriction triggers the rapid attachment and accumulation of neutrophils and monocytes to the endothelium, which is crucial for development of thrombosis (30). The process of neutrophil attachment to the endothelium and platelet-neutrophil interaction is predominantly mediated by selectin and integrin activation (16, 45, 46). Endothelial cells express the β_1 and β_2 integrin ligands ICAM1 and VCAM1, which are particularly abundant under inflamed conditions (16, 47, 48). To investigate whether inflammatory cytokines, which are commonly elevated in JAK2-V617F–induced disease, may modulate ICAM1 and VCAM1 expression, we tested HUVECs in response to TNF-α and IL-6 stimulation using flow cytometry. Strong upregulation of both ICAM1 and VCAM1 was detected in TNF-α–stimulated cells (Figure 5A), whereas IL-6 appeared to selectively induce ICAM1 expression (our unpublished observations). Of note, expression of E- and P-selectins was not affected by TNF-α and IL-6 (our unpublished observation). Thus, we hypothesized that in JAK2-V617F–induced disease increased ICAM1 and VCAM1 expression on endothelial cells in combination with abnormal β_1 and β_2 activity may precipitate abnormal adhesion of granulocytes to endothelial cells, contributing to pathologic thrombus formation. To study the role of β_1 and β_2 integrins in this process, we employed a widely used thrombosis model of the IVC (49). We induced thrombosis in JAK2$^{+/+}$ and JAK2$^{+/VF}$ mice by partial ligation of the IVC and 4 hours thereafter analyzed thrombus size and dry weight of the thrombi (Figure 5B).

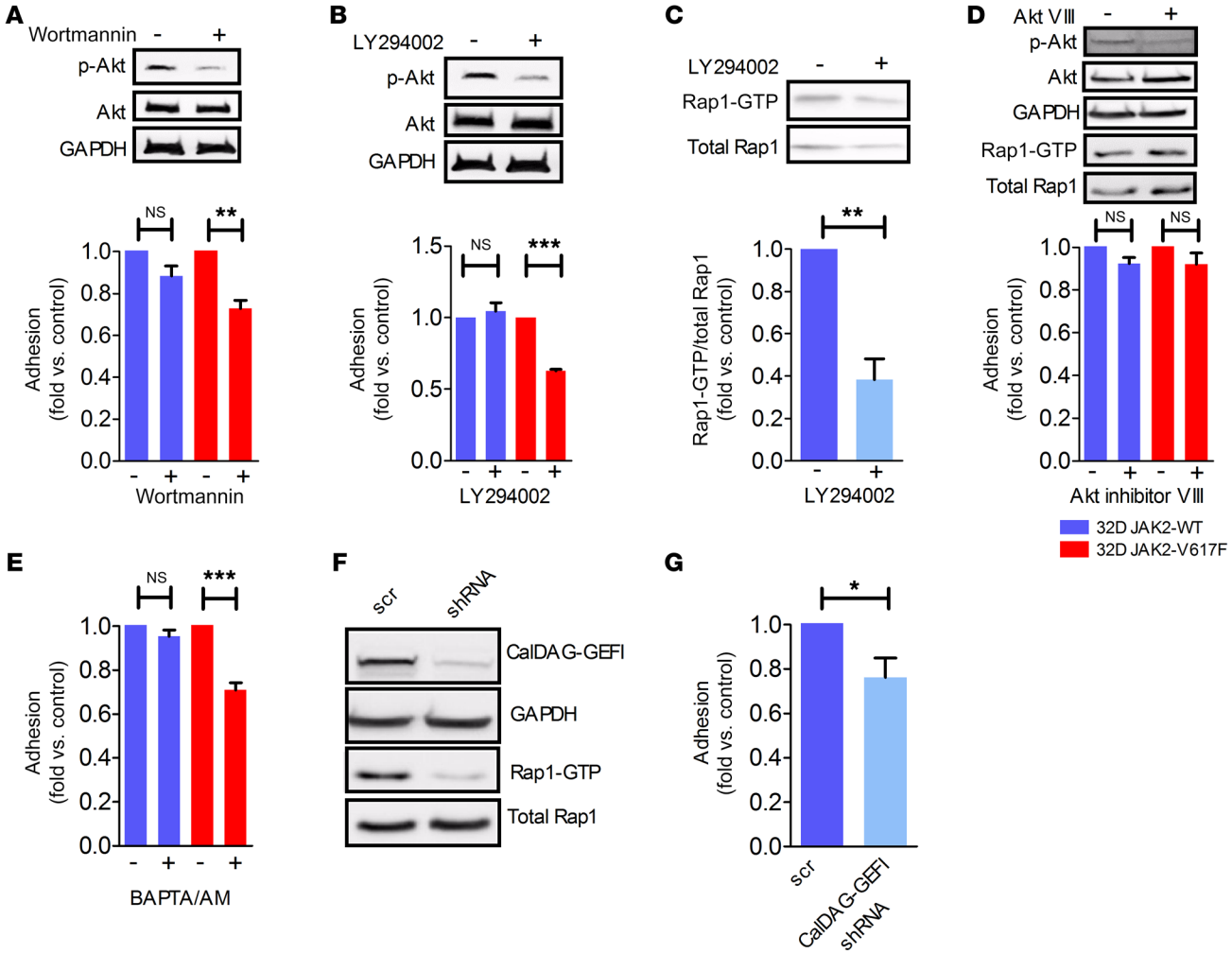

Figure 4. PI3K and CalDAG-GEFI are involved in Rap1 activation. Static adhesion on immobilized VCAM1 in the presence of (**A**) wortmannin (10 nM, 30 minutes) or (**B**) LY294002 (25 μM; 3 hours) in 32D JAK2-V617F and JAK2-WT cells. Minus symbol (–) indicates DMSO control. Representative Western blots (of 3 independent experiments) of phospho-Akt and Akt demonstrate the efficient blockade of signaling. (**C**) Inhibition of Rap1 activation by LY294002 treatment (25 μM; 3 hours) in 32D JAK2-V617F cells. Lower panel shows quantitative analysis of Rap1 activation given as fold compared with controls and corrected for loading variations using total Rap1; minus symbol (–) indicates DMSO control. (**D**) Rap1 pull-down and static adhesion on immobilized VCAM1 in the absence and presence of Akt inhibitor VIII treatment (0.5 μM; 4 hours) in 32D JAK2-V617F and JAK2-WT cells; minus symbol (–) indicates DMSO control. Representative Western blots (of 3 independent experiments) of phospho-Akt and Akt demonstrate the efficient blockade of signaling. (**E**) Static adhesion of 32D JAK2-V617F and JAK2-WT cells on immobilized VCAM1 in the absence and presence of BAPTA/AM (10 μM; 1 hour). (**F**) Static adhesion on immobilized VCAM1 of 32D JAK2-V617F cells transfected with scrambled (scr) or CalDAG-GEFI shRNA. (**G**) Rap1 pull-down after knockdown of CalDAG-GEFI results in reduced Rap1 activity. Data are shown as mean ± SEM. $^{*}P \le 0.05$, $^{**}P \le 0.01$, $^{***}P \le 0.001$ (1-way ANOVA with Bonferroni's post test and unpaired, 2-tailed Student's *t* test). Three independent experiments were performed each.

A significant increase in thrombus size and dry weight was observed in JAK2$^{+/VF}$ as compared with JAK2$^{+/+}$ mice, confirming previous reports on accelerated thrombosis in JAK2-V617F mice (50). Next, we determined the relative contribution of β_1 and β_2 integrin activity to JAK2-V617F–induced thrombus formation. JAK2$^{+/VF}$ mice were i.v. injected either with a combination of blocking antibodies against VLA-4 and β_2 integrins or with the corresponding isotype controls (Figure 5C). JAK2$^{+/VF}$ mice treated with VLA-4/β_2 integrin blocking antibodies showed dramatically reduced thrombus dry weight and size as compared with isotype control–injected JAK2$^{+/VF}$ mice. Thus, upon VLA-4/β_2 integrin blockade, JAK2$^{+/VF}$ mice displayed thrombus weight and size similar to those observed in JAK2$^{+/+}$ mice without VLA-4/β_2 integrin blockade. Together, these results uncover a crucial role of β_1/β_2 integrin overactivation in pathologic thrombus formation in JAK2-V617F–driven disease.

Spleen microenvironment and interaction with integrin ligands VCAM1 and ICAM1. In JAK2$^{+/VF}$ mice, development of CMN-like disease goes along with formation of splenomegaly and with effacement of the normal architecture of the spleen (34, 51). In order to analyze the changes in structure and cellular composition of JAK2$^{+/+}$ and JAK2$^{+/VF}$ spleens, we employed multi-epitope ligand cartography (MELC). This includes an analysis of VCAM1 and ICAM1, which are known to be expressed in the spleen (50, 51). Using this sequential automated multiparameter microscopy approach (52), we were able to characterize splenic architecture as well as cellular distributions and interactions by spatially resolved marker phenotypes (Figure 6, A–F; and

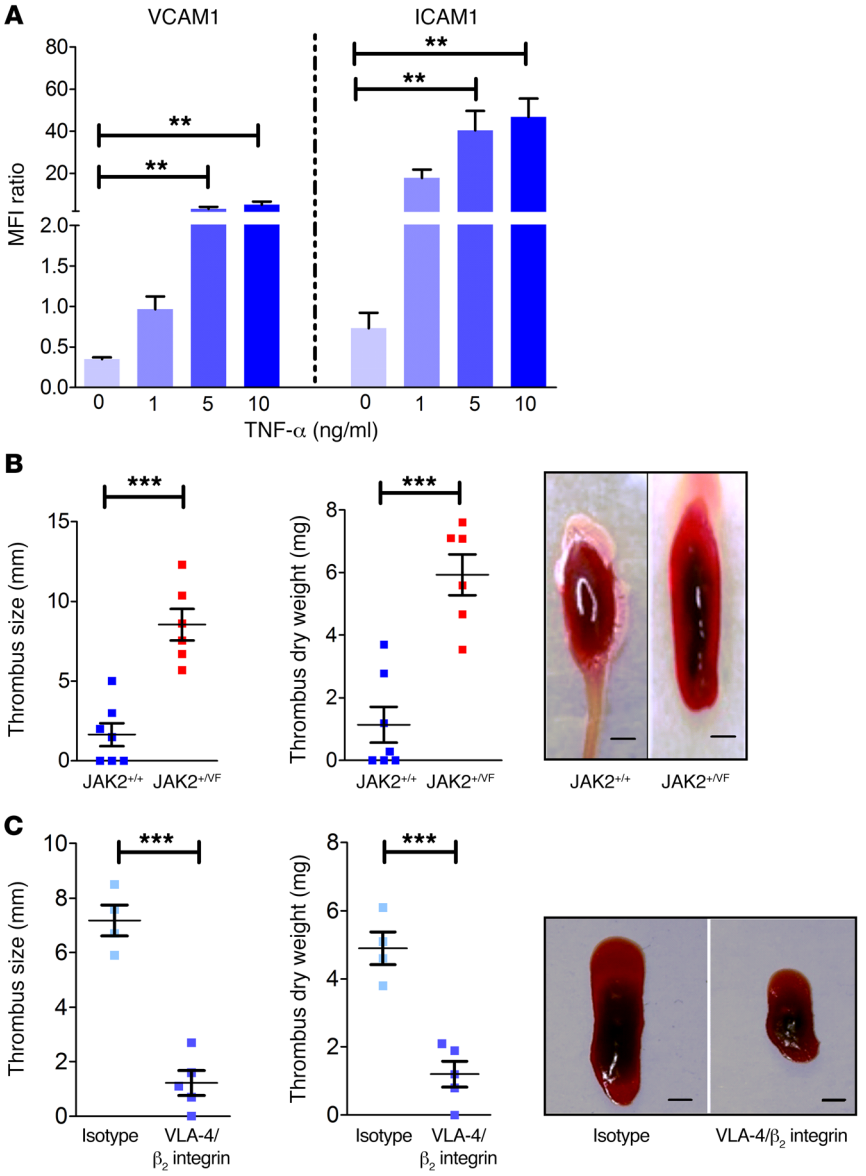

Figure 5. β_1 and β_2 integrin activity plays a major role in thrombosis formation. (**A**) HUVECs were stimulated with different concentrations (1, 5, and 10 ng/ml) of TNF-α for 24 hours. Flow cytometric analysis was performed for CD54 (ICAM1) and CD106 (VCAM1) expression (n = 6). (**B**) Partial ligation of IVC in 10- to 12-week-old JAK2$^{+/+}$ (n = 7) and JAK2$^{+/VF}$ (n = 6) mice results in increased thrombus size and dry weight in JAK2-V617F–positive mice. Representative images of isolated thrombi (scale bars: 1 mm). (**C**) JAK2$^{+/VF}$ mice were treated with VLA-4/β_2 integrin blocking antibodies (n = 5) or isotype control (n = 4) before partial ligation of IVC. Representative images of isolated thrombi (scale bars: 1 mm). Data are shown as mean ± SEM. $^{**}P \le 0.01$, $^{***}P \le 0.001$ (1-way ANOVA with Bonferroni's post test and unpaired, 2-tailed Student's t test).

and with the trend toward higher ICAM1 and VCAM1 expression in the white pulp, we found that the strict segregation of neutrophils almost exclusively located in the red pulp in JAK2$^{+/+}$ mice was lost in the JAK2$^{+/VF}$ animals, with the neutrophil density decreased in the red pulp and strongly increased in the white pulp (Figure 6, D and E; and Supplemental Figure 5A). In order to determine changes in the interaction of myeloid cells with VCAM1 and ICAM1, we employed a small object segregation approach by which the marker expression in proximity of VCAM1 and ICAM1 could be quantified (Supplemental Figure 5B). We found that the signal of CD11b in objects with direct contact to both VCAM1 and ICAM1 was significantly increased in the white pulp of JAK2$^{+/VF}$ mice (Figure 6F), indicating preferential binding of neutrophils to VCAM1 and ICAM1. Taken together, these data suggest that in addition to increased integrin activation in granulocytes, changes in splenic structure and disturbed expression of VCAM1 and ICAM1 might contribute to the altered distribution of these cells in the spleen.

Activated β_1 and β_2 integrins of JAK2-V617F–positive granulocytes stimulate abnormal trafficking to the spleen in vivo. In JAK2-V617F–positive disease in mice and humans, abnormal accumulation of mature myeloid cells characterized by expression of Gr-1 and CD11b and extramedullary granulopoiesis within the splenic cords has been observed (31, 34). Because MELC analysis demonstrated disturbed expression of VCAM1 and ICAM1 and altered distribution of granulocytes, we hypothesized that trafficking of myeloid cells into the spleen might be affected. Therefore, in vivo cell tracking was performed using whole-body single-photon emission computed tomography (SPECT) (Figure 7A). ^{111}Indium-labeled whole bone marrow (WBM) cells of JAK2$^{+/VF}$ or JAK2$^{+/+}$ mice (3×10^6 cells for each replicate) were injected into JAK2$^{+/+}$ recipients, and the distribution in the body was measured after 1 hour and 18 hours. In the early SPECT images obtained 1 hour after injection of JAK2$^{+/VF}$ or JAK2$^{+/+}$ cells, ^{111}indium was found predominantly in the blood pool (our unpublished observations), whereas after 18 hours the greatest ^{111}indium activity was found in liver and spleen. Interestingly, the amounts of ^{111}indium in spleen were substantially greater in mice injected with JAK2$^{+/VF}$ cells (Figure 7A, left panel). Standardized uptake values for the spleen were 15.1 for mice injected with JAK2$^{+/VF}$ cells and 9.7 for JAK2$^{+/+}$ cells (Figure 7A, right panel). To investigate which cell types preferentially home to the spleen, we injected WBM cells obtained from JAK2$^{+/+}$ or JAK2$^{+/VF}$ mice (carrying the congenic marker CD45.2) into CD45.1 recipients, and after 16 hours we analyzed the CD45.2-positive cell population in spleens. Strikingly, a higher pro-

our unpublished observations). A massive effacement of the typical JAK2$^{+/+}$ structure divided into red pulp, white pulp, and marginal zone was detected in JAK2$^{+/VF}$ spleens. However, for comparability of MELC results between JAK2$^{+/+}$ and JAK2$^{+/VF}$, we specifically searched for fields of view that presented residual white pulp structures (Figure 6A). Analysis for VCAM1 and ICAM1 revealed strong expression in JAK2$^{+/+}$ as well as in JAK2$^{+/VF}$ spleens (Figure 6B), although expression levels of both VCAM1 and ICAM1 were decreased in the red pulp of JAK2$^{+/VF}$ mice but increased in the white pulp and marginal zone (Figure 6C). In line with the disturbed splenic architecture

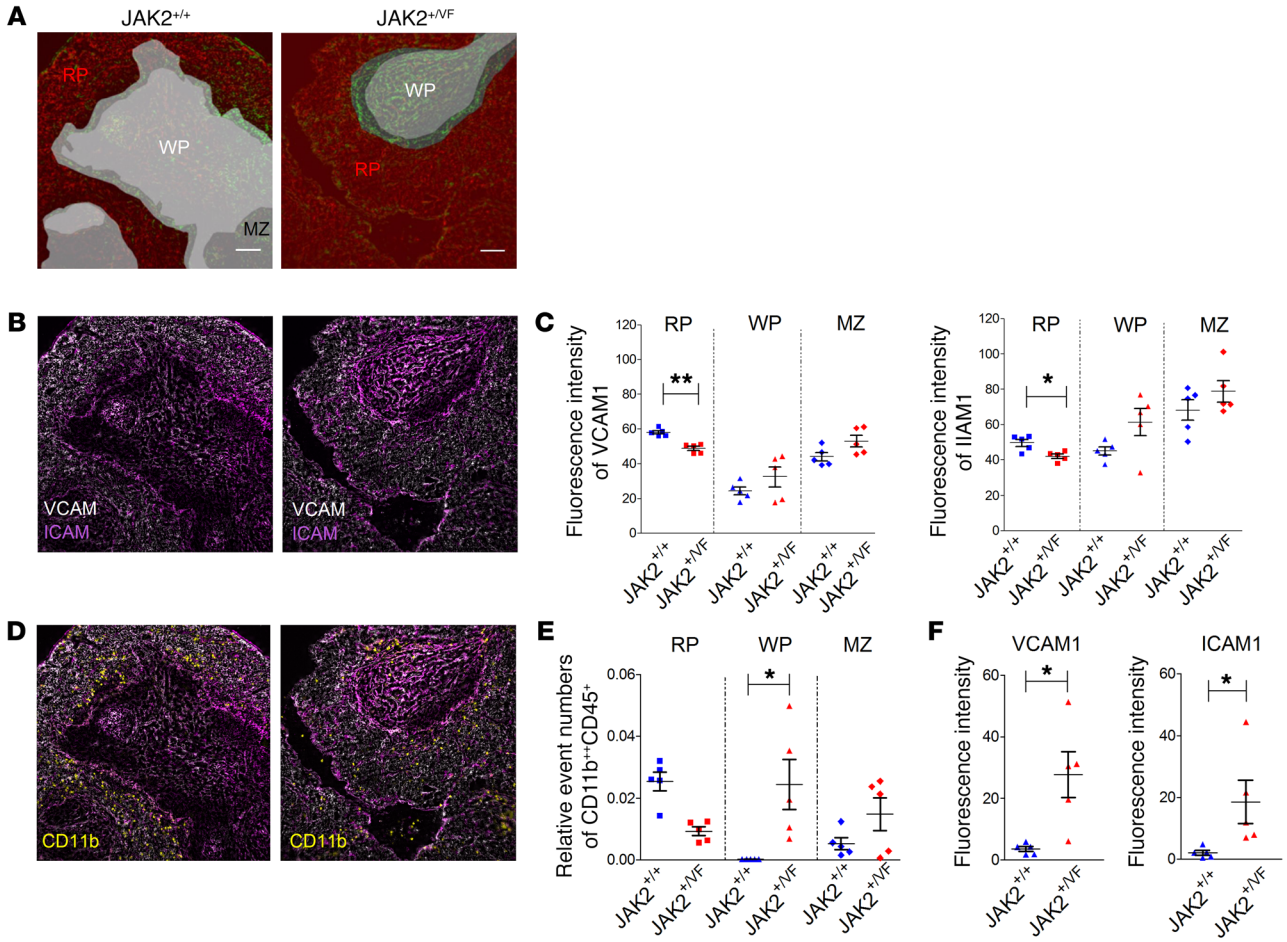

Figure 6. MELC of JAK$^{+/+}$ and JAK2$^{+/VF}$ spleens. (**A**) Segmentation of JAK2$^{+/+}$ (n = 5) and JAK2$^{+/VF}$ (n = 5) splenic tissue of into red pulp (RP), white pulp (WP), and marginal zone (MZ) based on the signals of VCAM1 and ICAM1. Scale bars: 50 μm. (**B**) Fluorescence signal of VCAM1 (white) and ICAM1 (magenta) for JAK$^{+/+}$ and JAK2$^{+/VF}$ spleen. (**C**) MFI of VCAM1 (left panel) and ICAM1 (right panel) for the regions defined in **A**. (**D**) The fluorescence signal of VCAM1 and ICAM1 was overlaid with the neutrophil marker protein CD11b. (**E**) Quantification of all neutrophils is depicted within the respective areas of the spleen based on fluorescence data shown in **D**. (**F**) MFI of CD11b signals in defined small objects that directly interact with VCAM1 (left panel) or ICAM1 (right panel). The definition of small objects is described in Supplemental Figure 5. An overlap of any small object of more than 0% and less than 20% with the regions positive for VCAM1 or ICAM1 is defined as directly interacting small object. Data were generated from 5 individual fields of view from 3 independent mice for each genotype. Horizontal bars represent the mean. *P < 0.05, **P < 0.01 (unpaired, 2-tailed Student's t test).

portion of granulocytes and monocytes from JAK2$^{+/VF}$ mice homed to the spleen as compared with cells derived from JAK2$^{+/+}$ littermate controls (Figure 7B). No differences could be observed in homing to the bone marrow (Supplemental Figure 6A). Integrins LFA-1 and VLA-4 together with chemokine receptor signaling mediate homing of leukocytes to the spleen (53). Therefore, bone marrow cells of JAK2$^{+/VF}$ mice were preincubated with a β_2 integrin blocking antibody or the corresponding isotype control before injection into CD45.1 recipients. This analysis revealed a reduced number of granulocytes and monocytes in the spleen (Figure 7C). In a stroke model, we have previously observed that neutrophil migration to the brain is dependent on VLA-4 (54). To investigate whether the increased homing ability correlates with constitutive activation of Rap1, we preincubated the bone marrow cells with the Rap1 inhibitor GGTI-2147 before injection into recipient mice. Inhibition of Rap1 suppressed abnormal splenic homing of injected JAK2-V617F–positive granulocytes and monocytes in vivo (Figure 7D) without having an apparent effect on cell survival (Supplemental Figure 6B). This finding is in line with studies highlighting that Rap1 activation and membrane relocalization are essential for β_1 integrin activation (38). Together the results suggest that increased β_1 and β_2 integrin activity drives abnormal trafficking and homing of granulocytes and monocytes to the spleen.

Discussion

As an initial approach to investigate the role of β_1 and β_2 integrins on leukocytes in CMN, we analyzed integrin expression in various leukocyte subsets isolated from JAK2$^{+/VF}$ knockin mice harboring physiologic expression of JAK2-V617F. Abundance of β integrins on the cell membrane among various leukocyte subsets was found to be differentially affected by JAK2-V617F. While β_1 integrin (CD29) expression in mouse and human (15) granulocytes was unchanged in the presence of JAK2-V617F, expression of β_2 integrins (CD18) was upregulated. These data are consistent with results of cDNA expression studies performed in granulocytes from JAK2-V617F–positive patients (55). Monocytes and T cells from JAK2$^{+/VF}$ knock-

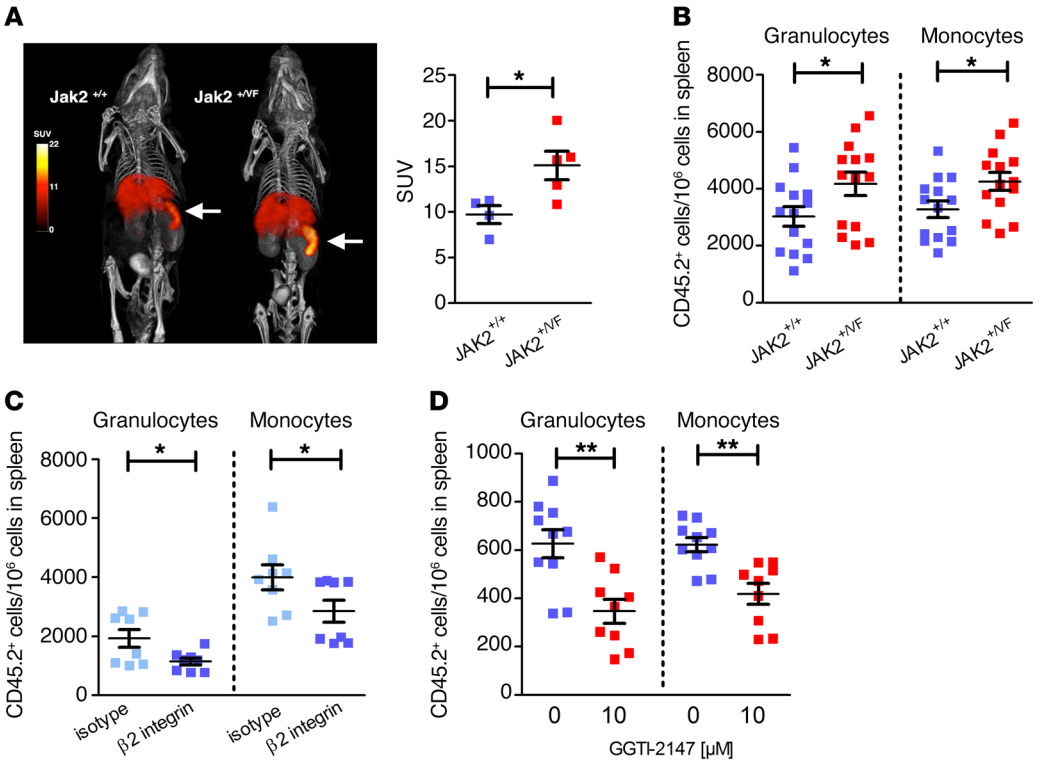

Figure 7. Increased adhesiveness and homing capacity to the spleen of primary JAK2$^{+/VF}$ murine myeloid cells. (**A**) Volume-rendered whole-body SPECT/CT images of a mouse injected with ^{111}indium-labeled JAK2$^{+/VF}$ WBM cells compared with a control mouse injected with ^{111}indium-labeled JAK2$^{+/+}$ cells. Representative SPECT images (pseudocolored) are overlaid on CT images (gray scale) (left panel). Mice were injected with a CT contrast agent. Units in the color scale for the SPECT images are standardized uptake values (SUV). SUV were 9.7 for mice (n = 4) injected with JAK2$^{+/+}$ cells compared with 15.1 for mice (n = 5) injected with JAK2$^{+/VF}$ cells (right panel). (**B**) WBM cells of 10- to 12-week-old JAK2$^{+/VF}$ or JAK2$^{+/+}$ mice (carrying the congenic marker CD45.2) were injected into CD45.1 recipient mice. Sixteen hours after injection, spleens of recipient mice were evaluated. Data represent number of detected CD45.2-positive granulocytes and monocytes per 10^6 cells in the spleen (n = 14/group) and are shown as mean ± SEM. *$P \le 0.05$ (unpaired, 2-tailed Student's t test). (**C**) Effect of β_2 integrin blocking antibody treatment (50 μg/ml; 30 minutes, n = 9) compared with isotype-treated cells (n = 10) on the number of detected CD45.2-positive granulocytes and monocytes per 10^6 spleen cells 16 hours after tail vein injection. (**D**) Effect of GGTI-2147 treatment (10 μM; 30 minutes) on the number of detected CD45.2-positive granulocytes and monocytes per 10^6 spleen cells 16 hours after tail vein injection (–GGTI-2147, n = 10 and +GGTI-2147, n = 9); 0 indicates DMSO control (left panel). Data shown as mean ± SEM. *$P \le 0.05$, **$P \le 0.01$ (nonparametric Mann-Whitney U test).

in mice displayed considerably higher membrane expression levels of both ICAM1 and VCAM1 in comparison to their counterparts isolated from JAK2$^{+/+}$ mice. Interestingly, single-cell expression profiling recently revealed that β_1 and β_2 integrins are subjects of regulation by JAK2-V617F at the level of hematopoietic stem cells in a murine model (56). As a functional consequence, upregulation of membrane expression may facilitate spontaneous and/or chemokine-induced clustering of integrins.

Regulation of integrin activation by chemokines/cytokines has been shown to depend on a plethora of inside-out signaling molecules (18, 19). Among the best-studied mechanisms is signaling via the small GTPases Rap1 and Rho. Rap1 activation and static adhesion on VCAM1 and ICAM1 are strongly enhanced in granulocytes from JAK2$^{+/VF}$ mice, confirming results obtained previously in human granulocytes from JAK2-V617F–positive patients and in 32D cells overexpressing JAK2-V617F (15). Recently, it has been demonstrated that signaling pathways of STAT3, STAT5, Akt, and ERK are constitutively activated by CALR mutations (57). However, we found no increase in Rap1 activation or ERK phosphorylation in CALR-positive human granulocytes as compared with JAK2-V617F–positive granulocytes. Thus, apparently, CALR-mutated cells exhibit differential signaling, which requires further investigation. Our findings are consistent with data suggesting a role for JAK2 in chemokine-induced Rap1 activation and integrin-mediated adhesion (58). Interestingly, excessive activation of Rap1 in a knockout model of SPA-1 showed development of a myeloproliferative-like disease and extramedullary hematopoiesis in the spleen (59), indicating an important role of Rap1 in initiation of the disease. Here we show that Rap1 activation in granulocytes is regulated by PI3K and CalDAG-GEFI activity. In ET, dysfunction of PI3K/Rap1 and of $\alpha_{IIb}\beta_3$ integrins results in hyperactivity of platelets (60). Furthermore, it was demonstrated that expression levels of CalDAG-GEFI correlate with β_3 integrin activation in megakaryocytes (61). In T cells, it was shown that CalDAG-GEFI and Rap1 regulate activation of LFA-1, whereas VLA-4 is activated by PLC and the PKC signaling pathway (62). In line with our results, Rap1 as well as β_1 and β_2 integrin activation are impaired in CalDAG-GEF$^{-/-}$ neutrophils (63). CalDAG-GEFI deficiency blocked adhesion to venules and migration into inflamed tissue and suppressed arterial thrombus formation in mice (63). Thus, PI3K and CalDAG-GEFI have been proposed as possible targets for future antithrombotic therapies (64, 65) blocking integrin activation of granulocytes and platelets.

Despite recent advances in understanding the pathophysiology of JAK2-V617F– induced CMN, the precise molecular mechanism that triggers the marked prothrombotic state — the primary cause of morbidity and mortality in patients with PV and ET — remains elusive (25). Interestingly, in elegant studies wherein $FeCl_3$ was used to occlude the carotid artery, tissue-specific expression of JAK2-V617F in megakaryocytes, and thus in platelets, failed to result in significant differences in occlusion time between WT and Pf4-Cre/FF1 mice (25). Moreover, membrane expression of integrin β_3, α_{IIb}, β_1, and α_2 was unchanged in resting platelets, and no significant differences were observed in the activity of the platelets as tested by P-selectin expression and activated $\alpha_{IIb}\beta_3$ levels (25). These results point to a minor role of platelets in JAK2-V617F–induced pathologic thrombus formation. The reticulocyte/erythrocyte compartment of $JAK2^{+/+}$ and $JAK2^{+/VF}$ mice expresses very low levels of CD29 (VLA-4) and of CD18 (LFA-1), which are barely detectable and apparently unchanged in $JAK2^{+/VF}$ mice (our unpublished observations). Thus, this finding argues against a major role of β_1 and β_2 integrins expressed on erythrocytes when inhibiting VLA-4/β_2 but points to the involvement of granulocytes and monocytes. Indeed in a recently published article, granulocytes were identified to play a pivotal role in venous thrombus formation in JAK2-V617F–knockin mice (66), supporting our finding that neutrophils are the major player in JAK2-V617F–driven thrombosis. The mechanism involved is increased formation of NETs (66, 67). Thus, that finding and the results presented here point to a scenario wherein increased Rap1 activation induced by JAK2-V617F results in increased adhesion of granulocytes to the endothelium, which in turn releases NETs, thereby triggering increased thrombus formation.

The occurrence of extramedullary hematopoiesis in the spleen of JAK2-V617F–positive CMN patients is associated with abnormal trafficking of hematopoietic cells, including clonal hematopoietic stem and progenitor cells. Our results employing SPECT analysis of ^{111}indium-labeled bone marrow cells isolated from $JAK2^{+/VF}$ mice show preferential binding of JAK2-V617F–positive hematopoietic cells to splenic structures. Recently, it has been shown that macrophages retain hematopoietic stem cells in the spleen via VCAM1 (68), providing a potential molecular mechanism operating in our model. Transplantation of CD45.2-positive bone marrow into CD45.1 recipient mice revealed that mature granulocytes and monocytes are clearly involved, albeit at low numbers. However, the follow-up time applied in our experiments was short (16 hours), and the cumulative nature of leukocyte trafficking to the spleen over time may translate into higher cell numbers. Nevertheless, there was a clear signal that granulocytes and monocytes from $JAK2^{+/VF}$ mice have an advantage in homing to the spleen, which is sensitive to β_2 integrin neutralization and to Rap1 inhibition by GGTI-2147. Abnormal interaction of JAK2-V617F–activated granulocytes and monocytes with splenic cells may contribute to an inflamed microenvironment, which may stimulate extramedullary hematopoiesis and thus splenomegaly. Although the exact molecular process is not entirely clear, it has already been proposed that potential mechanisms likely include differential responses to the unique splenic microenvironment of JAK2-V617F–positive disease (31, 34). Along this line, a striking change in the relative proportion of immune cells as granulocytes, monocytes, B cells, and T cells in the spleen of murine JAK2-V617F–positive disease has been described (31). Granulocyte trafficking between blood and tissue is primarily driven by selectins and integrins and their ligands expressed in tissue (69). Using MELC technology, we demonstrated high expression of VCAM1 and ICAM1 in splenic tissues from $JAK2^{+/+}$ and $JAK2^{+/VF}$ mice. As compared with other cells types, the numbers of JAK2-V617F–positive neutrophils were strongly increased in the white pulp of $JAK2^{+/VF}$ mice and revealed enhanced binding to VCAM1 and ICAM1.

In conclusion, our data show that JAK2-V617F activates intracellular signaling of β_1 and β_2 integrins in leukocytes. Our results have potentially broad implications, as they show that blocking integrin activation suppresses pathologic thrombus formation in a JAK2-V617F–positive mouse model. Thus, modulation of VLA-4 and LFA-1 integrin activity may constitute a potential future therapeutic approach for thrombosis in CMN patients refractory to standard treatment.

Methods

Mouse models. $JAK2^{+/VF}$ mice were provided by Ann Mullally (Division of Hematology, Department of Medicine, Brigham and Women's Hospital, Harvard Medical School, Boston, Massachusetts, USA) and have been characterized in detail (36). Floxed heterozygous $JAK2^{+/floxP\text{-}VF\text{-}floxP}$ animals were crossed with Vav-1-Cre transgenic mice (The Jackson Laboratory) (70) to induce hematopoietic JAK2-V617F expression starting during mouse embryogenesis. To rule out any secondary effects of Cre recombinase, $JAK2^{+/+}$ (Cre^+) and $JAK2^{+/VF}$ (Cre^+) mice were VavCre positive. Cre-mediated excision was verified by PCR using primers GACCAGTTGCTCCAGGGTTA, GCAAAGGGAGACAAGAAACGT, and TCACAAGCATTTGGTTTTGAAT. Blood was collected into EDTA-coated containers and analyzed on an ADVIA 2120 (Siemens Healthcare).

Cell culture. Murine promyeloid 32D cells (Leibniz Institute DMSZ–German Collection of Microorganisms and Cell Cultures) or Ba/F3 pro-B cells (ATCC) were stably transfected with EpoR and either JAK2-WT or JAK2-V617F and were cultured in RPMI 1640 medium supplemented with 10% FBS and 25 U/ml penicillin/streptomycin. For starvation, cells were cultured for 4 hours in serum-reduced (0.5%) medium at a density of 1×10^6 cells/ml. Starved cells were treated with GGTI-2147 (10 μM, 30 minutes), PI3K inhibitor LY294002 (25 μM, 3 hours) or wortmannin (10 nM, 30 minutes), Akt inhibitor VIII (0.5 μM; 4 hours), BAPTA/AM (10 μM; 1 hour). HUVECs (PromoCell) were cultivated with EndoPAN 3 medium (PAN Biotech) supplemented with 3% FBS, 10 nM L-glutamine, 0.75 U/ml heparin, 5 ng/ml hr-EGF, 5 ng/ml hFGF-2, 5 ng/ml VEGF, 50 μg/ml ascorbic acid sulphate, 15 ng/ml hr-IGF-1. Cells were seeded into 6-well plates and stimulated for 24 hours with 1, 5, and 10 ng/ml human TNF-α. Expression of VCAM1 (CD106; clone 51-10C9, BD Biosciences, catalog 555647) and ICAM1 (CD54; clone HA58, BD Bioscience, catalog 559771) was evaluated by flow cytometry. Median fluorescence intensity (MFI) ratio was calculated using MFI of specific antibody staining subtracted by MFI of the corresponding isotype control.

RNAi. For knockdown of CalDAG-GEFI, the pLKO.1 vector system with a puromycin resistance gene containing one shRNA sequence for CalDAG-GEFI (Sigma-Aldrich) was used. To generate lentiviral particles, HEK293T cells (Leibniz Institute DMSZ–German Collection of Microorganisms and Cell Cultures) were transfected using FuGENE HD Transfection Reagent (Promega). The knockdown efficiency was assessed by immunoblotting.

GTPase assays. Rap1 activation was determined using pull-down assays with commercially available kits (Active Rap1 Pull-Down and Detection Kit, Thermo Fisher Scientific) according to the manufacturer's instructions.

Isolation of granulocytes. Bone marrow was isolated from JAK2$^{+/VF}$ or JAK2$^{+/+}$ mice following standard procedures. Isolation of granulocytes was performed as described previously (71) with minor modifications. Lineage depletion (Supplemental Table 1) was performed using streptavidin particles. Purity was determined by fluorescence staining with Gr-1 and F4/80 antibodies.

Heparin-anticoagulated blood was obtained from healthy volunteers or untreated JAK2-V617F–positive or CALR-positive CMN patients (Supplemental Table 2). Samples were drawn after written informed consent was obtained. Mononuclear cells were removed by Ficoll-Paque density gradient centrifugation, followed by lysis of erythrocytes with BD FACS Lysing Solution (BD Biosciences).

Flow cytometry and antibody staining. The antibodies used for cell surface staining are described in Supplemental Table 1. Cells were stained in PBS containing 1% FBS for 1.5 hours at 4°C. SYTOX Blue Dead Cell Stain (Life Technologies) was used to exclude dead cells. Flow cytometry was performed on a FACSCanto II cytometer (Becton Dickinson). Expression of integrins was measured as MFI.

Integrin activation assay. Integrin activation assay was performed, as previously described, with minor changes (72). Murine granulocytes (1×10^6) were resuspended in ice-cold HBSS/1% FBS and incubated with 9EG7 antibody (CD29, clone 9EG7, BD Biosciences, catalog 553715) for 60 minutes at 4°C. Cells were washed and incubated with secondary antibody coupled to R-phycoerythrin (1:100) (clone Poly4054, BioLegend, catalog 405406) for 30 minutes at 4°C. Binding 9EG7 was expressed as MFI, represented in the graphs in relation to total CD29 (clone HMβ1-1, BioLegend, catalog 102215) expression.

Ligand binding assay. Murine granulocytes (1×10^6) were incubated in the absence or presence of recombinant soluble VCAM1/Fc or ICAM1/Fc (10 μg/ml, R&D Systems) for 60 minutes at 37°C. Cells were washed with ice-cold HBSS/1% FBS, followed by incubation with allophycocyanin-conjugated AffiniPure F(ab′)$_2$ fragment goat anti-human IgG, Fc-gamma fragment specific (1:100, 30 minutes, 4°C) (Dianova, catalog 109-136-098), and analyzed by flow cytometry. Binding of soluble ligand was expressed as MFI, calculated as fold of control relative to WT.

Homing assay. Bone marrow was isolated from 10- to 12-week-old JAK2$^{+/VF}$ or JAK2$^{+/+}$ mice as described previously (73). WBM cells (3×10^6) from JAK2$^{+/VF}$ or JAK2$^{+/+}$ mice (carrying the congenic marker CD45.2) were injected into CD45.1 (B6.SJL-*Ptprc^a Pepc^b*/Boy) recipient mice. Sixteen hours after injection, recipient mice were sacrificed and spleens were evaluated. Cells were stained with respective antibodies (Supplemental Table 1), and the amount of CD45.2-positive/10^6 cells in the myeloid compartment (monocytes Gr-1$^+$ and F4/80$^+$; granulocytes Gr-1$^+$) of the spleen was determined. Prior to homing assays, WBM cells from JAK$^{+/VF}$ mice were incubated with the Rap1 inhibitor GGTI-2147 (10 μM) for 30 minutes at 37°C or β_2 integrin blocking antibody (50 μg/ml, CD18; clone GAME46, BD Biosciences, catalog 555280), followed by injection into CD45.1 recipient mice as indicated.

Adhesion assay. Adhesion assays were performed as described previously (74). Black 96-well microplates were precoated with recombinant Fc-free murine VCAM1 and ICAM1 (Leinco Technologies) (3 μg/ml) or BSA. Granulocytes were incubated with LY294002 (25 μM, 3 hours), wortmannin (10 nM, 1 hour), BAPTA/AM (10 μM, 1 hour), or GGTI-2147 (10 μM, 30 minutes) at 37°C. Cells were labeled with calcein AM (2 μM) and allowed to adhere for 30 minutes at 37°C. Fluorescence of the samples was monitored during washing steps using a Synergy HT plate reader (BioTek).

Apoptosis assay. Isolated bone marrow cells from 10- to 12-week-old JAK2$^{+/VF}$ mice were incubated with or without 10 μM GGTI-2147 for 30 minutes, then washed twice with PBS. Cells were incubated in culture medium supplemented with IL-3 (6 ng/ml), IL-6 (10 ng/ml), murine stem cell factor (50 ng/ml), and thrombopoietin (10 ng/ml) and cultured for 16 hours, followed by annexin V/SYTOX Blue staining according to the manufacturer's instructions; and apoptosis was determined by flow cytometry.

Immunocytochemistry. Serum-starved 32D JAK2-WT and JAK2-V617F cells were plated on VCAM1-coated glass slides and incubated for 30 minutes at 37°C. Cells were washed with ice-cold PBS and fixed in 3.5% paraformaldehyde (15 minutes), followed by permeabilization with 0.1% Tween-20 (10 minutes) and blocking with 5% horse serum (15 minutes) at room temperature. For detection of Rap1, cells were incubated with mouse anti-Rap1 (clone 3/Rap1, BD Biosciences, catalog 610195) overnight at 4°C, followed by staining with Alexa Fluor 488–conjugated anti-mouse secondary antibody (Dianova, catalog 115-135-207). Actin was visualized by staining with APC-labeled phalloidin (Thermo Fisher Scientific, catalog 12379), and the nucleus was stained with DAPI (AppliChem). Fluorescence images were acquired with a Leica LSM SP5 and processed using NIH ImageJ software.

Subcellular fractionation. Serum-starved 32D cells (5×10^6) were subjected to subcellular fractionation using a commercially available kit (ProteoExtract Subcellular Proteome Extraction Kit, Calbiochem), according to the manufacturer's instructions.

Plasma membrane isolation. Serum-starved 32D cells (5×10^7) were subjected to plasma membrane isolation as previously described (75). As a control for enrichment in plasma membrane, the plasma membrane marker Na^+/K^+ ATPase (Cell Signaling Technology, catalog 3010) was used in immunoblot analysis.

Immunoblotting. Cell lysis and immunoblotting were performed as previously described (39). Na^+/K^+ ATPase (catalog 3010; 1:1,000), Akt (catalog 9272; 1:1,000), phospho-Akt (catalog 9271; 1:1,000), phospho-ERK (catalog 4370; 1:1,000), and ERK (catalog 9102; 1:1,000) antibodies were purchased from Cell Signaling Technology; β-actin antibody (catalog A5441; 1:10,000) was from MilliporeSigma, GAPDH antibody (catalog H86504M, 1:5,000) from Meridian Life Science, HDAC antibody (catalog sc-81598; 1:1,000) from Santa Cruz Biotechnology Inc., CalDAG-GEFI antibody (catalog ab137608; 1:1,000) from Abcam, and Rap1 antibody (catalog 16120; 1:1,000) from Thermo Fisher Scientific.

Partial ligation of the IVC. Ten- to 12-week-old JAK2$^{+/+}$ or JAK2$^{+/V617F}$ mice were anesthetized with sodium, ketamine (100 mg/kg body weight, i.p.), and xylazine (10 mg/kg body weight, i.p.) and placed on a 37°C thermostatically controlled operating platform. After laparotomy, sterile saline was applied to the exteriorized intestine to prevent drying. The IVC was gently separated from the aorta, and partial ligation (stenosis) was induced by placing a 30-gauge needle on the vessel and closure using a 7-0 polypropylene suture, followed by immediate removal of the needle. All visible side branches were ligated as well. After surgery, peritoneum and skin were closed with continuous 4-0 polypropylene sutures. All animals received subcutaneous analgesic (0.1 mg/kg buprenorphine) after

surgery. Four hours after partial ligation of the IVC, thrombi that developed below the suture were analyzed for size and weight. For blockade of integrins, a mixture of 200 μg VLA-4 antibody (clone PS/2, Hölzel Diagnostics, catalog BE0071) and 200 μg CD18 antibody (clone GAME46, BD Biosciences, catalog 555280) was injected i.v. 30 minutes before induction of partial IVC ligation.

In vivo cell tracking using ^{111}indium SPECT. CD45.1 recipient mice (10 weeks old) were i.v. injected with either JAK2$^{+/VF}$ or JAK2$^{+/+}$ WBM cells labeled with ^{111}indium according to the manufacturer's instructions (Mallinckrodt Pharmaceuticals). Labeling efficiency was 74.6% ± 6.6% for JAK2$^{+/VF}$ and 67.5% ± 8.4% for JAK2$^{+/+}$ cells. 5×10^6 cells were labeled with 50 MBq ^{111}indium. Mice were i.v. (jugular vein catheter) injected with ^{111}indium-labeled cells at a rate of 40 μl/min using perfusion pumps (76). For the first 2 animals (one JAK2$^{+/VF}$, one JAK2$^{+/+}$) syringes with 50 MBq were prepared; for the remaining animals, half the dose was used, as signal/noise ratios were high. After injection, the amounts of ^{111}indium in the syringes used for injection and in the tubes used for connecting syringes and catheters were determined with a radionuclide calibrator (Aktivimeter Isomed 2010). The injected dose was calculated by subtracting these remaining amounts of ^{111}indium from the amounts present in the syringe before injection.

For SPECT/CT imaging, animals were anesthetized with isoflurane (Baxter GmbH) and O_2 (induction 2.5% isoflurane and 0.8 l/min O_2; maintenance 1.2% isoflurane and 0.75–0.8 l/min O_2). Coregistered SPECT/CT scans were made using a 4-head NanoSPECT/CT (Mediso). Whole-body SPECT scans were made using apertures with nine 1.4-mm pinholes, providing a nominal spatial resolution of ≤1.0 mm. Acquisition times were 45 minutes to 1 hour. Photo peaks were set to the manufacturer's default values for ^{111}indium (171 keV ± 5% and 245 keV ± 5%). Reconstructions were made with isotropic voxel sizes of 300 μm. Whole-body CT scans were made at 45 keV, 0.17 mA, acquisition times of ca. 3.5–4.5 minutes depending on body size, 100 μm resolution; and reconstructed at isotropic voxel sizes of 200 μm using InVivoScope (version 1.43) software. Imeron 300 M (Bracco Imaging) was used as contrast agent and i.v. injected through the jugular vein catheter (500 μl at a rate of 50 μl/min) before the last CT scan after the final SPECT scan.

The data were analyzed using the OsiriX DICOM Viewer (version 5.7.1), Imaris software (x64, version 7.7.2, Bitplane), and Microsoft Excel (version 10.7.2). Whole-body ^{111}indium contents were quantified in OsiriX. Standardized uptake values for the spleen were calculated for each animal (^{111}indium content per cm^3 spleen divided by whole-body ^{111}indium content per whole-body volume in cm^3).

Automated multidimensional fluorescence microscopy by MELC. MELC was performed as described previously (52). Briefly, snap-frozen splenic tissues from JAK$^{+/+}$ and JAK2$^{+/VF}$ mice (16 weeks old) were embedded into O.C.T. (Sakura Finetek). 10-μm cryosections adhered to silane-coated cover slides were fixed with 2% paraformaldehyde, permeabilized with 0.2% Triton X-100, and blocked with 1% BSA/PBS. The tissue samples were transferred to an inverted wide-field fluorescence microscope (Leica DMI6000, ×20 air lens, NA 0.70). The automated cyclic robotic process started with the incubation of the first fluorescent antibody (tag) (Supplemental Table 1). After a series of washing steps, the fluorescence signals and a corresponding phase contrast image were acquired by a cooled charge-coupled device camera (Apogee KX4, Apogee Instruments). The specific signal of the given tag was removed by bleaching the fluorescent dye, followed by recording of post-bleaching fluorescence signals and repetition of the incubation-imaging-bleaching cycle. The appropriate working dilutions, incubation times, and positions within the MELC experiment were validated systematically using conditions suitable to MELC (52). The series of fluorescence images produced by each tag were aligned pixel-wise using the corresponding phase contrast images. The automated algorithm reaches an alignment accuracy of 0.1 pixels. Illumination faults of the images were corrected using flat-field correction. Post-bleaching images were subtracted from the following fluorescence tag images. Section artifacts were excluded as invalid by a manual mask-setting process. For intensity-based analysis or spatial distribution or relation of the recorded marker signals, we randomly segmented the multiparametric MELC image into small objects of a size of 16 pixels (Supplemental Figure 5A). For each of these small objects, the MFI and the smallest distance to 2 reference object masks were calculated. These masks were automatically created for the ICAM1 and VCAM1 marker signals to define regions that were positive for ICAM1 or VCAM1. The resulting matrix of intensities and distances was exported into a flow cytometry standard (FCS) file and uploaded to the online cytometry analysis platform Cytobank (https://www.cytobank.org/) for multiparametric analysis.

Statistics. Statistical significance was determined using an unpaired 2-tailed *t* test, nonparametric Mann-Whitney *U* test, or 1-way ANOVA. A *P* value less than 0.05 was considered significant.

Study approval. Mice were housed under specific pathogen–free conditions in the accredited Animal Research Facility of the Otto-von-Guericke University Medical Faculty, Magdeburg, Germany. All experiments were conducted with approval of the regional government authority Saxony-Anhalt (42502-2-1281, 42502-2-1112, and 42502-2-1133). Heparin-anticoagulated blood was drawn after written informed consent was obtained. Experiments were performed according to the guidelines of the Declaration of Helsinki and were approved by the Ethics Committee of the Medical Faculty Magdeburg (protocol MD115108).

Author contributions

BE, NG, TMS, JG, LP, KS, AMO, SW, FCS, SCN, PM, AG, JM, and HA performed experiments, analyzed data, and contributed to writing of the manuscript. DW, BI, and FHH provided essential materials. BE, NG, SK, RBD, HA, BS, AJM, FHH, and TF designed the research, analyzed data, and wrote the manuscript.

Acknowledgments

The authors thank Ann Mullally, Division of Hematology, Department of Medicine, Brigham and Women's Hospital, Harvard Medical School, for providing the JAK2$^{+/VF}$ knockin mouse. We also are grateful to Corinna Fahldieck, Stephanie Frey, Uta Schönborn, Anja Sammt, Annette Pethe, and Guido Höbbel (Otto-von-Guericke University) for expert technical assistance. We thank Andreas Fenske and Rainer Matthias (Otto-von-Guericke University) for support with the mouse experiments and Roland Hartig (Otto-von-Guericke University) for support with cell sorting. This project was supported by a grant from the German Research Council (DFG; SFB854, 2014-2017, and 2018-2021 to TF, FHH, RBD, SK, AJM, and BS), in part by grants from the José Carreras Foundation (DJCLS F 12/06 to FHH; SP 12/04 to FHH, in support of the Hematology Tumor Bank Magdeburg), by the German Ministry of Education and Research (BMBF; e.bio JAK-Sys to TF),

and by the Else-Kröner-Fresenius Foundation (Else-Kröner Forschungskolleg Magdeburg to TF and FHH). FHH was supported in part by the Thuringian state program ProExzellenz (RegenerAging — FSU-I-03/14) of the Thuringian Ministry for Research (TMWWDG).

Address correspondence to: Thomas Fischer, Department of Hematology and Oncology, Center for Internal Medicine, Otto-von-Guericke University Medical Center, Leipzigerstrasse 44, 39120 Magdeburg, Germany. Phone: 49.391.67.13266; Email: thomas.fischer@med.ovgu.de.

1. James C, et al. A unique clonal JAK2 mutation leading to constitutive signalling causes polycythaemia vera. *Nature*. 2005;434(7037):1144–1148.
2. Kralovics R, et al. A gain-of-function mutation of JAK2 in myeloproliferative disorders. *N Engl J Med*. 2005;352(17):1779–1790.
3. Levine RL, et al. Activating mutation in the tyrosine kinase JAK2 in polycythemia vera, essential thrombocythemia, and myeloid metaplasia with myelofibrosis. *Cancer Cell*. 2005;7(4):387–397.
4. Harrison C, et al. JAK inhibition with ruxolitinib versus best available therapy for myelofibrosis. *N Engl J Med*. 2012;366(9):787–798.
5. Verstovsek S, et al. Safety and efficacy of INCB018424, a JAK1 and JAK2 inhibitor, in myelofibrosis. *N Engl J Med*. 2010;363(12):1117–1127.
6. Quintás-Cardama A, Kantarjian H, Cortes J, Verstovsek S. Janus kinase inhibitors for the treatment of myeloproliferative neoplasias and beyond. *Nat Rev Drug Discov*. 2011;10(2):127–140.
7. Lussana F, Caberlon S, Pagani C, Kamphuisen PW, Büller HR, Cattaneo M. Association of V617F Jak2 mutation with the risk of thrombosis among patients with essential thrombocythaemia or idiopathic myelofibrosis: a systematic review. *Thromb Res*. 2009;124(4):409–417.
8. Tefferi A, Elliott M. Thrombosis in myeloproliferative disorders: prevalence, prognostic factors, and the role of leukocytes and JAK2V617F. *Semin Thromb Hemost*. 2007;33(4):313–320.
9. De Grandis M, et al. JAK2V617F activates Lu/BCAM-mediated red cell adhesion in polycythemia vera through an EpoR-independent Rap1/Akt pathway. *Blood*. 2013;121(4):658–665.
10. Hobbs CM, et al. JAK2V617F leads to intrinsic changes in platelet formation and reactivity in a knock-in mouse model of essential thrombocythemia. *Blood*. 2013;122(23):3787–3797.
11. Kleppe M, et al. JAK-STAT pathway activation in malignant and nonmalignant cells contributes to MPN pathogenesis and therapeutic response. *Cancer Discov*. 2015;5(3):316–331.
12. Falanga A, et al. Polymorphonuclear leukocyte activation and hemostasis in patients with essential thrombocythemia and polycythemia vera. *Blood*. 2000;96(13):4261–4266.
13. Falanga A, Marchetti M, Vignoli A, Balducci D, Barbui T. Leukocyte-platelet interaction in patients with essential thrombocythemia and polycythemia vera. *Exp Hematol*. 2005;33(5):523–530.
14. Alvarez-Larrán A, et al. Increased platelet, leukocyte, and coagulation activation in primary myelofibrosis. *Ann Hematol*. 2008;87(4):269–276.
15. Gupta N, et al. JAK2-V617F activates β1-integrin-mediated adhesion of granulocytes to vascular cell adhesion molecule 1. *Leukemia*. 2017;31(5):1223–1226.
16. Marino F, et al. Characterization of human leukocyte-HUVEC adhesion: effect of cell preparation methods. *J Immunol Methods*. 2017;443:55–63.
17. Panés J, Perry M, Granger DN. Leukocyte-endothelial cell adhesion: avenues for therapeutic intervention. *Br J Pharmacol*. 1999;126(3):537–550.
18. Hogg N, Patzak I, Willenbrock F. The insider's guide to leukocyte integrin signalling and function. *Nat Rev Immunol*. 2011;11(6):416–426.
19. Kinashi T. Intracellular signalling controlling integrin activation in lymphocytes. *Nat Rev Immunol*. 2005;5(7):546–559.
20. Ley K, Laudanna C, Cybulsky MI, Nourshargh S. Getting to the site of inflammation: the leukocyte adhesion cascade updated. *Nat Rev Immunol*. 2007;7(9):678–689.
21. Mitroulis I, Alexaki VI, Kourtzelis I, Ziogas A, Hajishengallis G, Chavakis T. Leukocyte integrins: role in leukocyte recruitment and as therapeutic targets in inflammatory disease. *Pharmacol Ther*. 2015;147:123–135.
22. Subramanian P, Mitroulis I, Hajishengallis G, Chavakis T. Regulation of tissue infiltration by neutrophils: role of integrin α3β1 and other factors. *Curr Opin Hematol*. 2016;23(1):36–43.
23. Wang J, Shiratori I, Uehori J, Ikawa M, Arase H. Neutrophil infiltration during inflammation is regulated by PILRα via modulation of integrin activation. *Nat Immunol*. 2013;14(1):34–40.
24. Hubbard AK, Rothlein R. Intercellular adhesion molecule-1 (ICAM-1) expression and cell signaling cascades. *Free Radic Biol Med*. 2000;28(9):1379–1386.
25. Etheridge SL, et al. JAK2V617F-positive endothelial cells contribute to clotting abnormalities in myeloproliferative neoplasms. *Proc Natl Acad Sci USA*. 2014;111(6):2295–2300.
26. Arellano-Rodrigo E, Alvarez-Larrán A, Reverter JC, Villamor N, Colomer D, Cervantes F. Increased platelet and leukocyte activation as contributing mechanisms for thrombosis in essential thrombocythemia and correlation with the JAK2 mutational status. *Haematologica*. 2006;91(2):169–175.
27. Arellano-Rodrigo E, et al. Platelet turnover, coagulation factors, and soluble markers of platelet and endothelial activation in essential thrombocythemia: relationship with thrombosis occurrence and JAK2 V617F allele burden. *Am J Hematol*. 2009;84(2):102–108.
28. Cervantes F, Arellano-Rodrigo E, Alvarez-Larrán A. Blood cell activation in myeloproliferative neoplasms. *Haematologica*. 2009;94(11):1484–1488.
29. Martinod K, Wagner DD. Thrombosis: tangled up in NETs. *Blood*. 2014;123(18):2768–2776.
30. von Brühl ML, et al. Monocytes, neutrophils, and platelets cooperate to initiate and propagate venous thrombosis in mice in vivo. *J Exp Med*. 2012;209(4):819–835.
31. Bumm TG, et al. Characterization of murine JAK2V617F-positive myeloproliferative disease. *Cancer Res*. 2006;66(23):11156–11165.
32. Passamonti F, et al. Prognostic factors for thrombosis, myelofibrosis, and leukemia in essential thrombocythemia: a study of 605 patients. *Haematologica*. 2008;93(11):1645–1651.
33. Passamonti F, et al. Relation between JAK2 (V617F) mutation status, granulocyte activation, and constitutive mobilization of CD34+ cells into peripheral blood in myeloproliferative disorders. *Blood*. 2006;107(9):3676–3682.
34. Prakash S, Hoffman R, Barouk S, Wang YL, Knowles DM, Orazi A. Splenic extramedullary hematopoietic proliferation in Philadelphia chromosome-negative myeloproliferative neoplasms: heterogeneous morphology and cytological composition. *Mod Pathol*. 2012;25(6):815–827.
35. Rosti V, et al. The expression of CXCR4 is down-regulated on the CD34+ cells of patients with myelofibrosis with myeloid metaplasia. *Blood Cells Mol Dis*. 2007;38(3):280–286.
36. Mullally A, et al. Physiological Jak2V617F expression causes a lethal myeloproliferative neoplasm with differential effects on hematopoietic stem and progenitor cells. *Cancer Cell*. 2010;17(6):584–596.
37. Rumi E, et al. JAK2 or CALR mutation status defines subtypes of essential thrombocythemia with substantially different clinical course and outcomes. *Blood*. 2014;123(10):1544–1551.
38. Medeiros RB, et al. Protein kinase D1 and the beta 1 integrin cytoplasmic domain control beta 1 integrin function via regulation of Rap1 activation. *Immunity*. 2005;23(2):213–226.
39. Schnöder TM, et al. Epo-induced erythroid maturation is dependent on Plcγ1 signaling. *Cell Death Differ*. 2015;22(6):974–985.
40. Schmid MC, Franco I, Kang SW, Hirsch E, Quilliam LA, Varner JA. PI3-kinase γ promotes Rap1a-mediated activation of myeloid cell integrin α4β1, leading to tumor inflammation and growth. *PLoS ONE*. 2013;8(4):e60226.
41. Wolf A, et al. JAK2-V617F-induced MAPK activity is regulated by PI3K and acts synergistically with PI3K on the proliferation of JAK2-V617F-positive cells. *JAKSTAT*. 2013;2(3):e24574.
42. Guidetti GF, Manganaro D, Consonni A, Canobbio I, Balduini C, Torti M. Phosphorylation of the guanine-nucleotide-exchange factor CalDAG-GEFI by protein kinase A regulates Ca(2+)-dependent activation of platelet Rap1b GTPase. *Biochem J*. 2013;453(1):115–123.
43. Arai A, Nosaka Y, Kanda E, Yamamoto K, Miyasaka N, Miura O. Rap1 is activated by erythropoietin or interleukin-3 and is involved in regulation of beta1 integrin-mediated hematopoietic cell adhesion. *J Biol Chem*. 2001;276(13):10453–10462.
44. de Rooij J, et al. Epac is a Rap1 guanine-nucleotide-exchange factor directly activated by cyclic AMP. *Nature*. 1998;396(6710):474–477.
45. Evangelista V, Manarini S, Coller BS, Smyth SS. Role of P-selectin, beta2-integrins, and Src tyro-

sine kinases in mouse neutrophil-platelet adhesion. *J Thromb Haemost*. 2003;1(5):1048–1054.
46. Zarbock A, Ley K. Mechanisms and consequences of neutrophil interaction with the endothelium. *Am J Pathol*. 2008;172(1):1–7.
47. Cook-Mills JM, Marchese ME, Abdala-Valencia H. Vascular cell adhesion molecule-1 expression and signaling during disease: regulation by reactive oxygen species and antioxidants. *Antioxid Redox Signal*. 2011;15(6):1607–1638.
48. Tosi MF, Stark JM, Smith CW, Hamedani A, Gruenert DC, Infeld MD. Induction of ICAM-1 expression on human airway epithelial cells by inflammatory cytokines: effects on neutrophil-epithelial cell adhesion. *Am J Respir Cell Mol Biol*. 1992;7(2):214–221.
49. Ponomaryov T, Payne H, Fabritz L, Wagner DD, Brill A. Mast cells granular contents are crucial for deep vein thrombosis in mice. *Circ Res*. 2017;121(8):941–950.
50. Lamrani L, et al. Hemostatic disorders in a JAK2V617F-driven mouse model of myeloproliferative neoplasm. *Blood*. 2014;124(7):1136–1145.
51. Marty C, et al. Myeloproliferative neoplasm induced by constitutive expression of JAK2V617F in knock-in mice. *Blood*. 2010;116(5):783–787.
52. Schubert W, et al. Analyzing proteome topology and function by automated multidimensional fluorescence microscopy. *Nat Biotechnol*. 2006;24(10):1270–1278.
53. Lo CG, Lu TT, Cyster JG. Integrin-dependence of lymphocyte entry into the splenic white pulp. *J Exp Med*. 2003;197(3):353–361.
54. Neumann J, et al. Very-late-antigen-4 (VLA-4)-mediated brain invasion by neutrophils leads to interactions with microglia, increased ischemic injury and impaired behavior in experimental stroke. *Acta Neuropathol*. 2015;129(2):259–277.
55. Rampal R, et al. Integrated genomic analysis illustrates the central role of JAK-STAT pathway activation in myeloproliferative neoplasm pathogenesis. *Blood*. 2014;123(22):e123–e133.
56. Lundberg P, et al. Myeloproliferative neoplasms can be initiated from a single hematopoietic stem cell expressing JAK2-V617F. *J Exp Med*. 2014;211(11):2213–2230.
57. Han L, et al. Calreticulin-mutant proteins induce megakaryocytic signaling to transform hematopoietic cells and undergo accelerated degradation and Golgi-mediated secretion. *J Hematol Oncol*. 2016;9(1):45.
58. Montresor A, Bolomini-Vittori M, Toffali L, Rossi B, Constantin G, Laudanna C. JAK tyrosine kinases promote hierarchical activation of Rho and Rap modules of integrin activation. *J Cell Biol*. 2013;203(6):1003–1019.
59. Ishida D, et al. Myeloproliferative stem cell disorders by deregulated Rap1 activation in SPA-1-deficient mice. *Cancer Cell*. 2003;4(1):55–65.
60. Moore SF, et al. Dysfunction of the PI3 kinase/Rap1/integrin α(IIb)β(3) pathway underlies ex vivo platelet hypoactivity in essential thrombocythemia. *Blood*. 2013;121(7):1209–1219.
61. Eto K, et al. Megakaryocytes derived from embryonic stem cells implicate CalDAG-GEFI in integrin signaling. *Proc Natl Acad Sci U S A*. 2002;99(20):12819–12824.
62. Ghandour H, Cullere X, Alvarez A, Luscinskas FW, Mayadas TN. Essential role for Rap1 GTPase and its guanine exchange factor CalDAG-GEFI in LFA-1 but not VLA-4 integrin mediated human T-cell adhesion. *Blood*. 2007;110(10):3682–3690.
63. Bergmeier W, et al. Mice lacking the signaling molecule CalDAG-GEFI represent a model for leukocyte adhesion deficiency type III. *J Clin Invest*. 2007;117(6):1699–1707.
64. Guidetti GF, Canobbio I, Torti M. PI3K/Akt in platelet integrin signaling and implications in thrombosis. *Adv Biol Regul*. 2015;59:36–52.
65. Stefanini L, Bergmeier W. CalDAG-GEFI and platelet activation. *Platelets*. 2010;21(4):239–243.
66. Wolach O, et al. Increased neutrophil extracellular trap formation promotes thrombosis in myeloproliferative neoplasms. *Sci Transl Med*. 2018;10(436):eaan8292.
67. Monti M, et al. Integrin-dependent cell adhesion to neutrophil extracellular traps through engagement of fibronectin in neutrophil-like cells. *PLoS One*. 2017;12(2):e0171362.
68. Dutta P, et al. Macrophages retain hematopoietic stem cells in the spleen via VCAM-1. *J Exp Med*. 2015;212(4):497–512.
69. Tecchio C, Cassatella MA. Neutrophil-derived chemokines on the road to immunity. *Semin Immunol*. 2016;28(2):119–128.
70. Georgiades P, et al. VavCre transgenic mice: a tool for mutagenesis in hematopoietic and endothelial lineages. *Genesis*. 2002;34(4):251–256.
71. Hasenberg M, et al. Rapid immunomagnetic negative enrichment of neutrophil granulocytes from murine bone marrow for functional studies in vitro and in vivo. *PLoS One*. 2011;6(2):e17314.
72. Rehberg K, et al. The serine/threonine kinase Ndr2 controls integrin trafficking and integrin-dependent neurite growth. *J Neurosci*. 2014;34(15):5342–5354.
73. Heidel FH, et al. The cell fate determinant Llgl1 influences HSC fitness and prognosis in AML. *J Exp Med*. 2013;210(1):15–22.
74. Kliche S, et al. CCR7-mediated LFA-1 functions in T cells are regulated by 2 independent ADAP/SKAP55 modules. *Blood*. 2012;119(3):777–785.
75. Kliche S, et al. The ADAP/SKAP55 signaling module regulates T-cell receptor-mediated integrin activation through plasma membrane targeting of Rap1. *Mol Cell Biol*. 2006;26(19):7130–7144.
76. Kolodziej A, et al. SPECT-imaging of activity-dependent changes in regional cerebral blood flow induced by electrical and optogenetic self-stimulation in mice. *Neuroimage*. 2014;103:171–180.